DOI: https://doi.org/10.15407/techned2020.06.069

INFLUENCE OF WINDING ENDS ON THE PARAMETERS OF PULSE INDUCTOR WITH U-SHAPED CORE

R.S. Kryshchuk*
Institute of Electrodynamics of National Academy of Sciences of Ukraine
Peremohy ave., 56, Kyiv, 03057, Ukraine, e-mail: dep7ied@ukr.net

It is known from the scientific literature that magnetic pulse processing of electrically conductive non-magnetic sheet materials helps to reduce residual stresses, especially in welded joints. This is due to magnetoplastic and electroplastic effects. To create such effects in non-magnetic electrically conductive materials with welded joints, an inductor with pulsed magnetic field, U-shaped magnetic circuit and hollow conductor for possibility of active cooling of the winding is proposed. Such inductor allows inducing high-density pulsed currents in electrically conductive non-magnetic sheet materials with welded joints. It studies the parameters of the inductor - active resistance and inductance in the frequency-domain mode. The parameters calculated in two-dimensional and three-dimensional models are compared. The electromagnetic field is calculated using Maxwell equations and finite element method. Parameters of an ends of winding are determined by the difference in the parameters of the three-dimensional and two-dimensional models of the induction system. Resistance is calculated separately in the groove`s part of the winding, the outer part and on the frontal parts. The parameters of the induction system with a ferromagnetic core and non-magnetic thin-sheet alloy AMg6 are calculated for various values of complex amplitude of current in winding. Additionally, the parameters are calculated both without the magnetic core and without the non-magnetic metal. The quantitative comparison of the parameters of the three-dimensional model with the two-dimensional one is performed. The active resistance and inductance of end parts of the inductor are investigated by well-known analytical expressions from handbooks of electric machines. References 11, figures 3, tables 6.
Key words: magnetic-pulse processing, U-shaped core, electromagnetic parameters, winding`s ends.

Magnetoplastic and electroplastic effects [1, 2] was found and investigated in the series non-magnetic crystals (NaCl, CsI, LiF, Zn, Al, Cu). These effects increase or decrease plastic property of materials, remove residual stresses in heterogeneous structure of materials, and change durability too.

Magnetoplastic effect in the materials with welding joints is caused by magnetic field. Electroplastic effect is caused by high density eddy currents. Magnetic field and induced currents can be direct, alternative, or pulsed. It is known about positive effect due to influence the pulsed electric currents $10^8 \ldots 10^9$ A/m^2 in electrically conductive materials [3]. In [4] there is that magnetic pulse processing increases fatigue strength of welded joints of AMg6 alloy [5]. It significantly reduces residual tensile stresses from 165 MPa and more while converting to compression stress 80 MPa [4]. Experimental results demonstrate significant decrease and redistribution of residual welding stresses in AMg6 alloy specimen after pulsed electromagnetic treatment [10]. Paper [6] presents an experimental study about effect by pulsed electromagnetic processing on fatigue resistance of aluminum (alloy 2011). Clear beneficial effect has been observed.

Inductors with pulsed magnetic field are proposed in the department of electromagnetic systems of the Institute of Electrodynamics of the National Academy of Sciences of Ukraine to create high density eddy currents in electrically conductive non-magnetic materials by non-contact method (Fig. 1) [11]. A magnetic U-shaped core (Fig. 1) allows concentrating eddy currents into narrower stream in an electrically conductive non-magnetic workpiece materials. Thus, greater local current density in welding joints (Fig. 1) can be achieved.

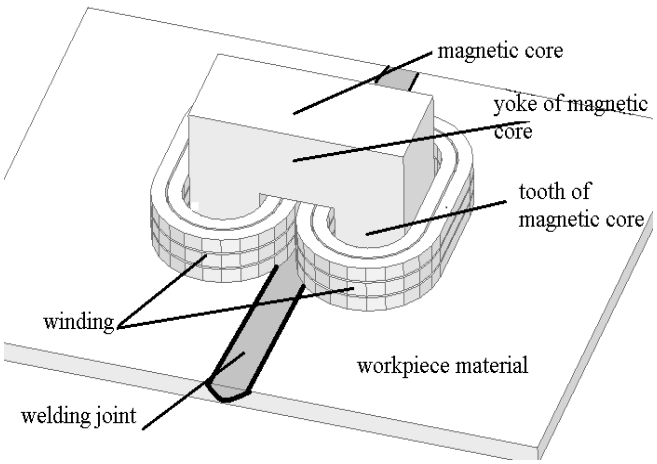

Fig. 1

*ORCID ID: https://orcid.org/0000-0002-1933-0144

Pulsed eddy currents 10^9 A/m^2 in a welding joint of sheet workpiece material (Fig. 1) is achieved by the pulsed current in a winding in form of a half-wave of a sine wave. Frequency-domain mode is used to calculate the resistance and inductance of the inductor (Fig. 1).

Modeling meets difficulty with the three-dimensional formulation (Fig. 2, *b*) due to requirement huge computational resources [11]. But the two-dimensional formulation (Fig. 2, *a*) requires less computational resources, has less computational time. The two-dimensional model of the inductor doesn't take into account winding ends. Therefore, there is the problem how to take into account the influence of winding's ends on the total active resistance R and inductance L of the inductor.

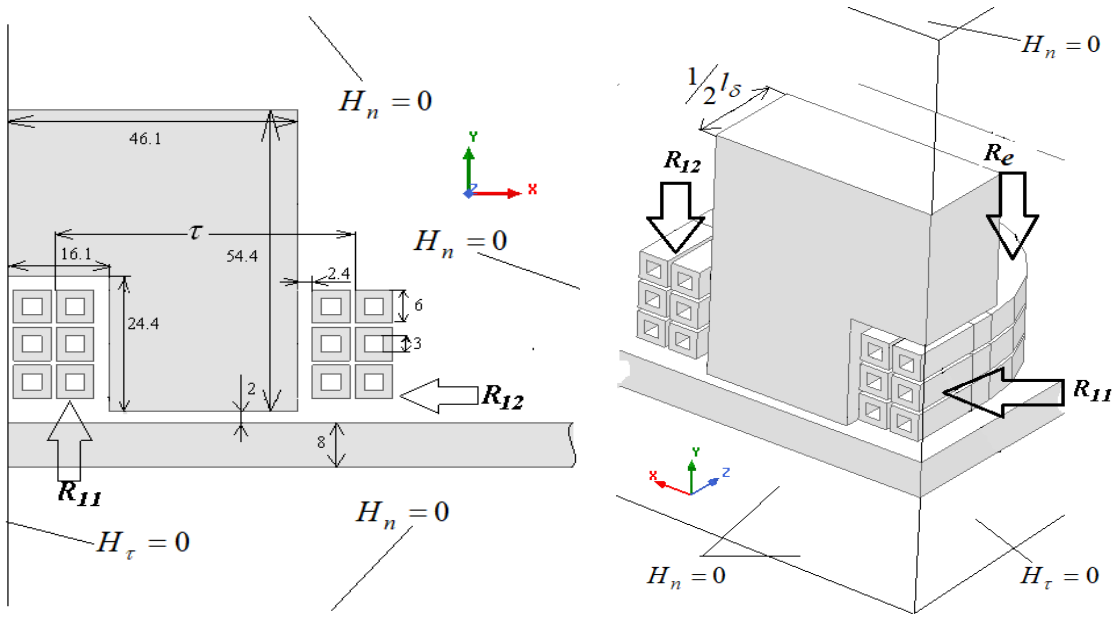

a *b*

Fig. 2

The aim is to investigate the parameters of the winding`s ends of the induction system with U-shaped magnetic core, two coils, tube winding and to investigate the adequacy of simple methods of bringing a results of the two-dimensional numerical model to the three-dimensional formulation.

To solve the problem, the inductor is modeled in two-dimensional and three-dimensional formulations (Fig. 2). The two-dimensional model (Fig. 2, *a*) represents 1/2 symmetrical part of the inductor with the length along z axis equals with length of magnetic core l_δ, and the three-dimensional model (Fig. 2, *b*) represents 1/4 symmetrical part of the inductor. For calculating magnetic field, the finite element method is used. The magnetization curve of the magnetic core is also taken into account (steel AISI-1010).

Equations of electromagnetic field in quasi-stationary mode:

$$div\mathbf{B} = 0,\quad rot\mathbf{H} = \mathbf{j},\quad rot\mathbf{A} = \mathbf{B},\quad rot\mathbf{E} = -\partial\mathbf{B}/\partial t,\quad \mathbf{E} = -\partial\mathbf{A}/\partial t - grad\phi,\quad \mathbf{B} = \mu\mathbf{H},\ \mathbf{j} = \sigma\mathbf{E}. \qquad (1)$$

There $\mathbf{A}$, $\mathbf{B}$, $\mathbf{H}$, $\mathbf{j}$ are the vectors of magnetic vector potential, magnetic induction, magnetic field strength, current density respectively; σ is the electrical conductivity; t is the time, φ is the electric scalar potential, μ is the magnetic permeability. For the frequency-domain mode, the equations (1) are change as follows:

$$div\hat{\mathbf{B}} = 0,\ rot\hat{\mathbf{H}} = \hat{\mathbf{j}},\ rot\hat{\mathbf{A}} = \hat{\mathbf{B}},\ rot\hat{\mathbf{E}} = -i\omega\hat{\mathbf{B}},\ \hat{\mathbf{E}} = -i\omega\hat{\mathbf{A}} - grad\varphi,\ \hat{\mathbf{B}} = \mu\hat{\mathbf{H}},\ \hat{\mathbf{j}} = \sigma\hat{\mathbf{E}}. \qquad (2)$$

There $\hat{\mathbf{A}}$, $\hat{\mathbf{B}}$, $\hat{\mathbf{H}}$, $\hat{\mathbf{j}}$ are the complex amplitudes of magnetic vector potential, magnetic induction, magnetic field strength, current density respectively, ω is the angular frequency, i is the imaginary unit.

According to the equations (2) the equation to calculate magnetic field for two-dimensional model (Fig. 2, *a*) is

$$rot(\mu^{-1} rot\hat{\mathbf{A}}) = -i\omega\sigma\hat{\mathbf{A}} + \hat{\mathbf{j}}_s. \qquad (3)$$

There $\hat{\mathbf{j}}_s$ is the current density complex amplitude of the source due to differences in electric potential at terminals. This current density $\hat{\mathbf{j}}_s$ is present in the cross section of each wire of winding.

Equation for three-dimensional model (Fig. 2, *b*) by the (2) is

$$rot\left(\sigma^{-1} rot\hat{\mathbf{H}}\right) = -i\omega\hat{\mathbf{B}} + rot\left(\sigma^{-1}\hat{\mathbf{j}}_s\right). \qquad (4)$$

The following boundary conditions are specified: at the external boundaries of the computational region (Fig. 2, *a* and *b*), and at the boundary of cross-section of wires of winding (Fig. 2, *b*) the normal magnetic field strength equals zero

$$H_n = 0; \tag{5}$$

on the border of cross-section of the yoke of magnetic core (Fig. 2, *a*, *b*) – the tangential component of magnetic field strength is zero

$$H_\tau = 0; \tag{6}$$

at the internal boundaries there is the boundary with equality of tangential components of magnetic field strength on both sides of each border

$$H_y^+ = H_y^- . \tag{7}$$

After solving equations (3) or (4) the averaged magnitude value of an induction is calculated in a tooth of a magnetic core (Fig. 1)

$$B_{avg} = \frac{1}{V}\int_V \left|\hat{\mathbf{B}}\right| dV , \tag{8}$$

where V is the volume of a tooth of a magnetic core.

Inductance of an inductor is evaluated by the average energy (W_{AV})

$$L = 4W_{AV}I_m^{-2} = I_m^{-2}\int_V \left(\left|\hat{\mathbf{B}}\right| \cdot \left|\hat{\mathbf{H}}\right|\right) dV . \tag{9}$$

Here I_m is the magnitude value of current in the winding.

The resistance R of an inductor consists with the resistance of a winding R_1, and the resistance from electrical losses in workpiece sheet metal R_2:

$$R = R_1 + R_2 . \tag{10}$$

The resistance R_1 can be divided into the following parts

$$R_1 = R_{11} + R_{12} + R_e , \tag{11}$$

where R_{11} is the resistance of winding in groove of magnetic core (Fig. 2), R_{12} is the out-of-groove winding resistance (Fig. 2), R_e is the resistance of end of winding in the 3D model (Fig. 2, ***b***). Each such part of the winding has its own AC resistance factor

$$k_r = R / R_{dc} . \tag{12}$$

R is the resistance of alternative current (R_{AC}), R_{dc} is the resistance of direct current.

Resistance in any region of the model (R_{AC}) is calculated by the expression

$$R = 2PI_m^{-2} . \tag{13}$$

There are electrical losses P, which are determined by integrating the power density over the volume V of each region of winding (Fig. 2)

$$P = \int_V P_V dV . \tag{14}$$

Power density P_V is calculated by expression

$$P_V = \left|\hat{\mathbf{j}}\right|^2 (2\sigma)^{-1} = \left|rot\hat{\mathbf{H}}\right|^2 (2\sigma)^{-1} . \tag{15}$$

There $\hat{\mathbf{j}}$ is the current density in volume of electric conductive region.

Magnetic force between the inductor and workpiece sheet metal which is directed along the y-axis is calculated by follow expression

$$F_y = \int_S T_{yy} dS = \int_S \mu_r\mu_0 \left(H_y^2 - 0{,}5\left|\mathbf{H}\right|^2 \right) dS . \tag{16}$$

There T_{yy} is the Maxwell tension tensor [8].

Table 1 presents calculation results of the two-dimensional (2D) model (Fig. 2, *a*) of the inductor. Length along axis *z* equals magnetic core length (l_δ = 100 mm).

Table 1

I_m, kA	2D model (l_δ =100 mm), Fig. 2, *a*						
	R_2, mohm	R_{11}, mohm	R_{12}, mohm	$\sum R$, mohm	F_y, kN	B_{avg}, T	L, uH
1	7,62	9,27	2,81	19,70	00,15	0,19	8,50
6	7,26	8,98	2,80	19,04	05,16	1,36	8,29
11	5,93	6,95	2,50	15,38	14,19	2,11	7,42
16	4,88	5,48	2,24	12,60	24,75	2,52	6,67
16 (without core)	2,19	2,73	1,75	6,670	11,12	-	4,15

Table 2

I_m, kA	3D model (l_δ =100 mm), Fig. 2, *b*								
	R_2, mohm	R_{11}, mohm	R_{12}, mohm	R_e, mohm	$\sum R$, mohm	F_y kN	B_{avg}, T	L, uH	L_e, uH
1	11,27	9,02	3,02	4,69	28,00	0,23	0,30	13,08	4,58
6	10,12	8,10	2,87	4,30	25,39	7,19	1,98	12,39	4,10
11	08,19	6,22	2,53	3,73	20,67	19,4	2,81	11,11	3,69
16	07,44	5,56	2,40	3,54	18,94	37,73	3,60	10,57	3,90
16 (without core)	03,03	2,61	1,73	2,82	10,19	15,46	-	6,37	2,22

Table 2 presents calculation results of the three-dimensional (3D) model (Fig. 2, *b*) of the inductor. It has magnetic core length l_δ =100 mm and other dimensions from Fig. 2, *a*. Inductance of winding's ends L_e of the 3D model is calculated by difference of 3D and 2D inductances L from tables 2 and 1:

$$L_e = L^{(3D)} - L^{(2D)}. \quad (17)$$

It should be emphasized that inductance L_e includes mutual inductance between ends of winding and main part of inductor.

Tables 3 and 4 are similar to tables 1 and 2, but the length of the core along z axis is l_δ = 40 mm.

Tables 5 and 6 presents calculation results of inductor without sheet workpiece material and with core length along *z* axis l_δ = 40 mm. Tables comparisons 5 and 6 with 3 and 4 let to see the effect of presence of the workpiece material on the parameters (resistance and inductance). In tables 5-6 there aren`t magnetic force F_y and resistance R_2 due to absence workpiece material under the inductor.

Tables 1-6 show how

Table 3

I_m, kA	2D model (l_δ =40 mm), Fig. 2, *a*						
	R_2, mohm	R_{11}, mohm	R_{12}, mohm	$\sum R$, mohm	F_y, kN	B_{avg}, T	L, uH
1	3,05	3,71	1,12	7,88	0,06	0,19	3,40
6	2,91	3,59	1,12	7,62	2,07	1,36	3,32
11	2,37	2,78	1,00	6,15	5,69	2,11	2,97
16	1,95	2,19	0,90	5,04	9,93	2,52	2,67

Table 4

I_m, kA	3D model (l_δ =40 mm), Fig. 2, *b*								
	R_2, mohm	R_{11}, mohm	R_{12}, mohm	R_e, mohm	$\sum R$, mohm	F_y kN	B_{avg} T	L, uH	L_e, uH
1	6,6	3,58	1,32	4,72	16,22	00,13	0,44	7,91	4,51
6	5,04	2,57	1,10	3,92	12,63	03,61	2,34	6,90	3,58
11	4,12	2,04	0,97	3,51	10,64	09,92	3,27	6,22	3,25
16	3,79	1,88	0,92	3,38	09,97	19,18	4,20	5,94	3,27

parameters change due to the saturation of the magnetic core by changing current at terminals. It is also shown that the 3D model has already saturated magnetic core at the current 6 kA, and the 2D model has similar saturation at the current 11 kA. Therefore, the equivalent 3D model can be obtained by increasing the length of the 2D model along z axis, but it will give some deviation.

Table 5

I_m, kA	2D model, Fig. 2, *a*						
	R_2, mohm	R_{11}, mohm	R_{12}, mohm	$\sum R$, mohm	F_y, kN	B_{avg}, T	L, uH
1	-	3,71	1,13	4,84	-	0,44	8,03
6	-	2,2	0,88	3,08	-	2,22	6,22
11	-	1,41	0,74	2,16	-	2,76	4,73
16	-	1,21	0,71	1,92	-	3,22	4,09

Table 6

I_m, kA	3D model, Fig. 2, *b*								
	R_2, mohm	R_{11}, mohm	R_{12}, mohm	R_e, mohm	$\sum R$, mohm	F_y kN	B_{avg}, T	L, uH	L_e, uH
1	-	3,59	1,46	4,59	9,64	-	0,82	15,79	7,76
6	-	1,60	0,89	3,19	5,68	-	3,02	10,61	4,39
11	-	1,36	0,82	3,03	5,21	-	4,38	09,47	4,74
16	-	1,28	0,79	2,99	5,06	-	5,75	09,03	4,94

In order to perform the calculation of an inductor in the 2D model and to get the result close to the result in the 3D model, 2D model can be calculated with the length along the z axis more than the length of the magnetic core. But it is necessary to find out by what dimension length along z axis the 2D model can be increasing.

The parameters of the 3D models (tables 2, 4, 6) of the inductor (Fig. 2, *b*) are divided on the parameters of its 2D model (tables 1, 3, 5) in order to find out how many times they differ (Fig. 3). This difference is the result of the presence of winding`s ends. In the Fig. 3 there are: inductance coefficient k_L; resistance coefficients k_R, k_{R1}, k_{R2}; magnetic force coefficient k_F; coefficient of averaged magnetic induction in teeth of magnetic core k_B:

$$k_L = L^{3D}/L^{2D}, \quad k_R = R^{3D}/R^{2D}, \quad k_{R1} = R_1^{3D}/R_1^{2D},$$
$$k_{R2} = R_2^{3D}/R_2^{2D}, \; k_F = F^{3D}/F^{2D}, \; k_B = B_{avg}^{3D}/B_{avg}^{2D}. \quad (18)$$

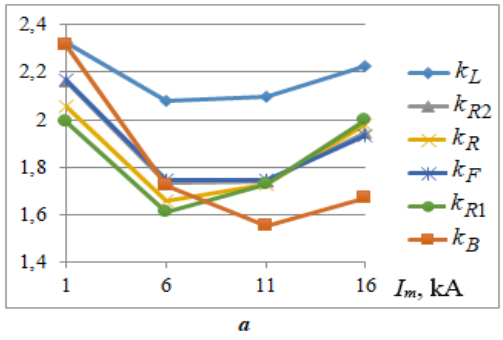

a

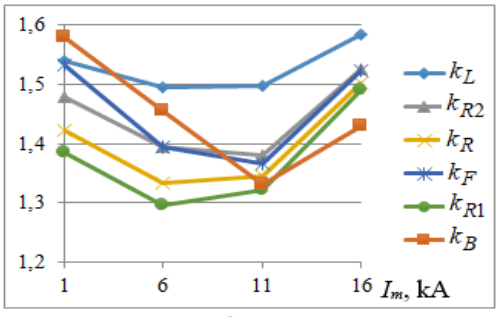

b

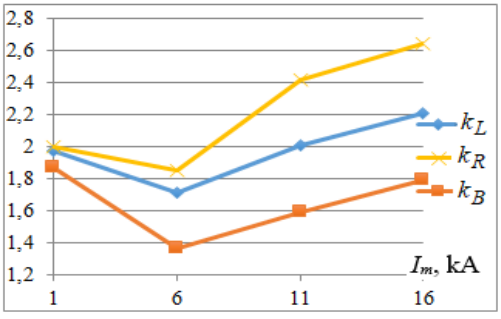

c

Fig. 3

On the Fig. 3, *a* there are coefficients obtained from tables 1 and 2. Averaged inductance coefficient $(k_L)_{avg}$ is 1,53; averaged resistance coefficient $(k_R)_{avg}$ is 1,43 of all of them (k_{R1} and k_{R2} are too); averaged force coefficient $(k_F)_{avg}$ is 1,43 that similar to resistance in this case.

Results without core are obtained for current 16 kA (Table 1, 2 with mark "without core") and not presented in the Fig. 3 because they do not change with increasing current. It`s inductance coefficient k_L is 1,53; resistance coefficient k_R is 1,43; force coefficient k_F is 1,39.

On the Fig. 3, *b* there are the same coefficients as on the Fig. 3, *a*, but with core length 40 mm, from the tables 4 and 5. Average inductance coefficient k_L is 2,2; averaged resistance k_R and force k_F coefficients are 1,9.

On the Fig. 3, *c* there are the same coefficients with core length 40 mm but without workpiece material under the core. Average inductance coefficient k_L is 1,97; average resistance coefficient k_R is 2,22.

It is also seen that the dependences in Fig. 3 have a nonlinear character – they have smaller values when the core transitions from the unsaturated state to the saturated state.

All parameters in 2D model can be reduced to parameters in 3D model with some deviation. The easiest way is increasing the estimated depth of the 2D model along axis *z* by more than the length of magnetic core l_δ (Fig. 2, *a*). Calculation results in the Fig. 3 show that averaged coefficients (18) can be obtained by increasing length of 2D model along *z* axis by the pole distance τ (Fig. 2, *a*):

$$k_L = k_R = k_{R1} = k_{R2} = k_F = k_B = (l_\delta + \tau) l_\delta^{-1}. \quad (19)$$

Then the depth of the two-dimensional model along the z axis should be set as

$$l'_\delta = l_\delta + \tau. \quad (20)$$

For example, if the magnetic core is 100 mm long along *z* axis (Table 1-2), and the pole distance τ is 47 mm (Fig. 2,a), then the parameters of the two-dimensional model (Table 1) are multiplied by a coefficient 1.47 (19) and compared with the parameters of the three-dimensional model (table 2). For example, for the current 6 kA with taking into account (20) the deviation for the active resistance is 10% compared with 3D model, for the inductance is 1.5%, for the induction in the teeth of the magnetic circuit is 1%, for the magnetic force is 5.4%.

Another way to bring the parameters of the 2D model of the inductor to equivalent 3D is using the analytical calculation of the inductance and the active resistance of end parts. In this case, the depth along the z axis of the 2D model is equal to the length of the core l_δ.

A well-known expression for calculating the inductance of the end parts of single-phase motors [7]

$$L_e = 4\pi f \mu_0 \frac{(wpq)^2}{pq} q(0{,}47 l_e - 0{,}3\tau). \quad (21)$$

Here, the number 4 means the number of end parts of the winding; μ_0 is the magnetic constant, w is the number of turns in each coil, p is the number of pole pairs, q is the number of grooves per pole and phase, l_e is the length of one winding's end, τ is the pole distance. For the inductor's models (fig. 2) two coils are included in series. And they can be represented as one coil with $2 \cdot w$ turns, number of pole pairs $p = 1/2$, number of grooves per pole and phase $q = 1$.

For the model in fig. 2 expression (21) gives the result L_e = 3.8 uH. This result is closer to the simulation results when using the workpiece material (tables 2, 4) with the averaged induction in the magnetic core 2...2.34 T. Deviation during this induction is not more than 10%. In the case without the workpiece material under the inductor (table 6), the inductance according to expression (21) gives 16% lower value. With the absence of the magnetic core, the inductance from the end parts is 2.22 uH (table 4), which is 1.7 times less in comparison with the analytical expression (21) (L_e = 3.8 uH).

Active resistance of the end parts R_e can be obtained approximately using a simple known analytical expression for calculating the active resistance of the wire with direct current

$$R_{dc} = l_w (\sigma s_w)^{-1}. \quad (22)$$

Here l_w is the length of the wire, σ is the electrical conductivity of the wire, s_w is the cross section of the wire. Then, to calculate the active resistance of end parts R_e the direct current resistance R_{dc} must be multiplied by the AC losses coefficient k_r (12).

Coefficient k_r (12) has the different value in different parts of the winding (Fig. 2, b): winding in groove (R_{11}); winding outside the groove (R_{12}), winding in the end parts (R_e). Using expression (22) and resistances R_{11}, R_{12}, R_e from tables 1-3 it is possible to obtain k_r in different parts of the winding. The calculation from tables 2, 4, 6 shows approximately the same values of the coefficient k_r in the resistances R_{12} and R_e. For example, in the inductor with the magnetic core length of 100 mm, and the amplitude value of the current 1 kA (table 2), these coefficients are equal to 3,4 and 3,58, respectively in R_{12} and R_e, and at the current of 11 kA they coincide and equal to 2,85.

A coefficient k_r in the end parts can be approximately produced by the expressions from [9]

$$k_r = \phi(\xi) + \frac{(m/2)^2 - 1}{3}\psi(\xi), \qquad \xi = h_w\sqrt{\frac{b_w n}{b_n + 1,2h_m}\pi f \mu_0 \sigma_{Cu}},$$

$$\phi(\xi) = \xi\frac{sh(2\xi) + \sin(2\xi)}{ch(2\xi) - \cos(2\xi)}, \qquad \psi(\xi) = 2\xi\frac{sh(\xi) - \sin(\xi)}{ch(\xi) + \cos(\xi)}. \tag{23}$$

Here b_n is the width of the cross section of the winding coils along the x axis (Fig. 2); h_m is the height of a cross section of a coil of a winding along the y axis; b_w is the width of a cross section of a conductor; h_w is the height of the cross section of a conductor; m and n are the number of layers of conductors of a coil section along the height (y axis) and width (x axis), respectively.

Expressions (23) gives the coefficient for the model in Fig. 2 equals to 2,86. This coefficient coincides with the value from table 2 at the current 11 kA (k_r = 2,85, B_{avg} = 3 T). For other current values (1, 6, 16 kA) this coefficient does not coincide exactly with the values from table 2. For example, at 1 kA (B_{avg} = 0,3 T), the deviation has its maximum value at 25%.

Conclusions.

• It is shown that the resistance and inductance of an induction system with a U-shaped magnetic circuit halve when the magnetic core is saturated. The parameters of an induction system depend nonlinearly on the magnitude of a current in windings.

• Reducing the parameters of the two-dimensional model to the three-dimensional one with a certain error (from 1% to 10%) is possible by setting the length (depth) of the two-dimensional model in this way: the length of a magnetic core plus the pole distance of winding coils.

• Calculation of the inductance of end parts by the well-known analytical expression for end parts of single-phase machines gives the deviation to 10% with the condition that averaged magnetic induction in the teeth of magnetic core is 2...2.4 T and with workpiece material under the core.

• The coefficient of increasing losses (AC losses) of end parts of the winding coincides with the analytically obtained one with the deviation to 5%.

• The calculation of the coefficient of increasing losses in end of winding is also possible with the well-known analytical expressions for electric machines. But these expressions show result with less deviation for the inductor with the saturated magnetic core (more than 3 T), and for the unsaturated magnetic core (0,3 T) – with the deviation 25 %.

Роботу виконано за рахунок коштів бюджетної програми «Надійність і довговічність матеріалів, конструкцій, обладнання та споруд» (КПКВК 6541030).

1. Kuznetsov N.N. The effect of electric and magnetic pulse effects on the workpiece. *Obrabotka materialov davleniem.* 2010. No 3(24). Pp. 126-129. (Rus)

2. Komshina AV., Pomelnikova A.S. Promising method of low-energy materials processing using a magnetic field. *Nauka i Obrazovanie.* 2012. No FC77 – 48211. Pp. 463-488. DOI: https://doi.org/10.7463/0912.0454270 (Rus)

3. Samokhvalov V.N., Samokhvalova Zh.V. Magnetic-pulse and electric pulse processing of machine parts. *Sovremennye problemy teorii mashyn.* 2017. No 5. Pp. 113-115. (Rus)

4. Lobanov L.M., Kondratenko I.P., Zhltsov A.V., Karlov O.M., Pashchyn M.O., Vasyuk V.V., Yashchuk V.A. Electrophysical unsteady processes in the system to reduce residual stresses welds *Tekhnichna elektrodynamika.* 2016. No 6. Pp. 10-19. DOI: https://doi.org/10.15407/techned2016.06.010 (Rus)

5. Database of Steel and Alloy (Marochnik)
URL: www.splav-kharkov.com/en/e_mat_start.php?name_id=1433 (accessed at 15.12.2019)

6. Mohin M.A., Toofanny H., Babutskyi A., Lewis A., Xu Y.G. Effect of electromagnetic processing on fatigue resistance of 2011 aluminum alloy *Journal of Multiscale Modeling*. 2016. Vol. 7. No 3. Article number 1650004. DOI: https://doi.org/10.1142/S1756973716500049

7. Kopylov I.P., Goryainov F.A., Klokov B.K., Morozkin V.P., Tokarev B.F. Design of electrical machines. Moskva: Enerhiia, 1980. 496 p. (Rus)

8. Tamm I.E. Theory of electricity. Moskva: Nauka, 1976. 616 p. (Rus)

9. Postnikov I.M. Electrical machinery design. Kiev: Gostekhizdat, 1962. 736 p. (Rus)

10. Stepanov G., Babutski A., Mameev I., Pashchin N., Savitskii V., Tkachuk G. Redistribution of residual welding stresses in pulsed electromagnetic treatment. *Strength of Materials.* 2011. No 43(3). Pp. 326-331.
DOI: https://doi.org/10.1007/s11223-011-9300-2

11. Rashchepkin A.P., Kondratenko I.P., Karlov A.N., Kryshchuk R.S. Electromagnetic field of W-shaped inductor for magnetic-pulse processing of materials *Tekhnichna Elektrodynamika.* 2019. No 6. Pp. 5-12.
DOI: https://doi.org/10.15407/techned2019.06.005 (Ukr)

УДК 620.171./1; 621.313; 536.2

ВЛИЯНИЕ ЛОБОВЫХ ЧАСТЕЙ НА ПАРАМЕТРЫ ИМПУЛЬСНОГО ИНДУКТОРА С П-ОБРАЗНЫМ МАГНИТОПРОВОДОМ

Р.С. Крищук, канд.техн.наук
Институт электродинамики НАН Украины,
пр. Победы, 56, Киев, 03057, Украина, e-mail: dep7ied@ukr.net

Известно, что магнитно-импульсная обработка электропроводящих немагнитных тонколистовых материалов помогает снизить остаточные напряжения, особенно в сварных соединениях. Это связано с магнитопластическим и електропластическим эффектами. Для создания таких эффектов в немагнитных электропроводящих материалах со сварными соединениями предложен индуктор с импульсным магнитным полем, П-образным магнитопроводом и с проводниками-трубками для возможности активного охлаждения обмотки. Такой индуктор позволяет индуцировать импульсные токи высокой плотности в электропроводящих немагнитных тонколистовых материалах со сварными соединениями. Исследуются параметры индуктора – активное сопротивление и индуктивность в квазистационарном режиме и режиме гармонических токов. Сравниваются параметры, рассчитанные в двумерной и трехмерной моделях. Электромагнитное поле рассчитывается с использованием уравнений Максвелла и метода конечных элементов. Параметры лобовых частей обмотки определяются разницей параметров трехмерной и двумерной моделей индукционной системы. Сопротивление рассчитывается в пазе, внешней части обмотки и на лобовых частях обмотки отдельно. Выполнен расчет параметров индукционной системы с ферромагнитным магнитопроводом и тонколистовым немагнитным сплавом АМг6 для различных значений комплексной амплитуды тока в обмотке. Дополнительно выполнен расчет параметров как без магнитопровода, так и без немагнитного обрабатываемого металла. Выполнено количественное сравнение параметров трехмерной модели с двумерной. Исследовано активное сопротивление и индуктивность лобовых частей индуктора, которые рассчитаны по известным аналитическими выражениями. Библ. 11, рис. 3, табл. 6.

Ключевые слова: электромагнитные параметры, П-образный магнитопровод, магнитопластичный эффект, електропластичный эффект.

УДК 620.171./1; 621.313; 536.2

ВПЛИВ ЛОБОВИХ ЧАСТИН НА ПАРАМЕТРИ ІМПУЛЬСНОГО ІНДУКТОРА З П-ПОДІБНИМ МАГНІТОПРОВОДОМ

Р.С. Крищук, канд.техн.наук
Інститут електродинаміки НАН України,
пр. Перемоги, 56, Київ, 03057, Україна, e-mail: dep7ied@ukr.net

Відомо, що магнітно-імпульсна обробка електропровідних немагнітних тонколистових матеріалів допомагає знизити залишкові напруження, особливо в зварних з'єднаннях. Це пов'язано з магнітопластичним і електропластичним ефектами. Задля створення таких ефектів в немагнітних електропровідних матеріалах зі зварними з'єднаннями пропонується індуктор з імпульсним магнітним полем, П-подібним магнітопроводом і з провідниками-трубками задля можливості активного охолодження обмотки. Такий індуктор дає змогу індукувати імпульсні струми високої щільності в провідних немагнітних тонколистових матеріалах зі зварними з'єднаннями. Досліджуються параметри індуктора – активний опір і індуктивність в квазістаціонарному режимі. Порівнюються параметри, що розраховані в двовимірній і тривимірній моделях. Електромагнітне поле розраховується з використанням рівнянь Максвелла і методу скінченних елементів. Параметри лобових частин обмотки визначаються різницею параметрів тривимірної і двовимірної моделей індукційної системи. Опір розраховується в пазі, зовнішньої частини обмотки і на лобових частинах обмотки окремо. Виконано розрахунок параметрів індукційної системи з феромагнітним магнітопроводом і тонколистовим немагнітним сплавом АМг6 для різних значень комплексної амплітуди струму в обмотці. Додатково виконано розрахунок параметрів як без магнітопроводу, так без немагнітного оброблюваного металу. Виконано кількісне порівняння параметрів тривимірної моделі з двовимірною. Досліджено активний опір і індуктивність лобових частин індуктора, що розраховані за відомими аналітичними виразами. Бібл. 11, рис. 3, табл. 6.

Ключові слова: електромагнітні параметри, П-подібний магнітопровід, магнітопластичний ефект, електропластичний ефект.

Надійшла: 08.01.2020
Остаточний варіант: 27.07.2020